IOPscience iopscience.iop.org

Home Search Collections Journals About Contact us My IOPscience

LISA Pathfinder drag-free control and system implications

This article has been downloaded from IOPscience. Please scroll down to see the full text article.

2005 Class. Quantum Grav. 22 S139

(http://iopscience.iop.org/0264-9381/22/10/002)

View the table of contents for this issue, or go to the journal homepage for more

Download details:
IP Address: 193.205.203.3
The article was downloaded on 27/03/2012 at 13:26

Please note that terms and conditions apply.

INSTITUTE OF PHYSICS PUBLISHING CLASSICAL AND QUANTUM GRAVITY

Class. Quantum Grav. **22** (2005) S139–S148 doi:10.1088/0264-9381/22/10/002

LISA Pathfinder drag-free control and system implications

Walter Fichter[1], **Peter Gath**[1], **Stefano Vitale**[2] **and Daniele Bortoluzzi**[2]

[1] EADS Astrium GmbH, Friedrichshafen, Germany
[2] University of Trento, Trento, Italy

E-mail: walter.fichter@astrium.eads.net

Received 10 November 2004, in final form 1 February 2005
Published 21 April 2005
Online at stacks.iop.org/CQG/22/S139

Abstract

The top-level requirement of the LISA Pathfinder mission is the verification of pure relative free fall between two test masses with an accuracy of about 3×10^{-14} m s^{-2} Hz$^{-1/2}$ in a measurement bandwidth between 1 mHz and 30 mHz. The drag-free control system is one of the key technology elements that shall be verified. Its design is strongly connected to the overall system and experimental design, in particular, via the following issues: the differential test mass motion and thus the science measurements depend on the control system; design constraints, such as negative stiffness of test masses and electrostatic actuation cross-talk, have an impact on science and control system performance; derived requirements for control system components, in particular, the micro-propulsion system, must be within reasonable and feasible limits. In this paper, the control design approach is outlined and the system-related issues are addressed.

PACS numbers: 07.87.+v, 02.30.Yy, 07.05.Dz

(Some figures in this article are in colour only in the electronic version)

1. Introduction

1.1. Science objective and sensitive axis control

The primary scientific objective of the LISA Pathfinder mission is the verification of pure gravitational free fall between two test masses within 3×10^{-14} m s^{-2} Hz$^{-1/2}$ $[1 + (f/3\ \text{mHz})^2]$ in a measurement bandwidth (MBW) between 1 mHz and 30 mHz. To this end, the relative displacement measurements between two test masses are provided by an optical metrology system, along the sensitive axis. Figure 1 shows a schematic view of the LISA Technology Package (LTP) consisting of the two test masses (TM1 and TM2), the optical bench, metrology system and the forces available and acting along the sensitive axis.

 © 2005 IOP Publishing Ltd Printed in the UK

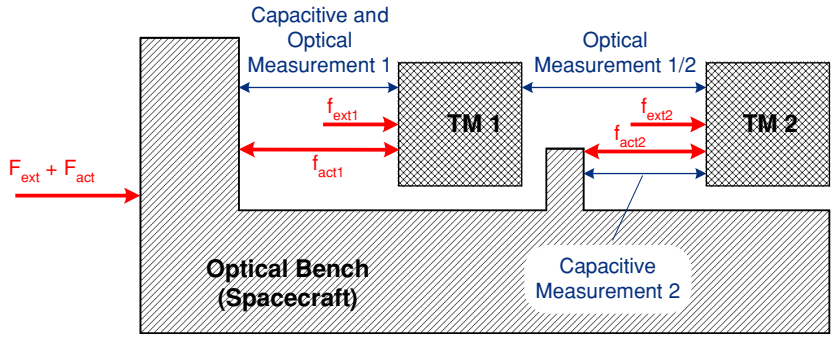


Figure 1. Schematic view of the spacecraft and the test masses along the sensitive axis.

In order to minimize the differential acceleration due to stiffness effects along the sensitive axis, the test masses have to stay centred with respect to their housings. This is accomplished by two control loops along the sensitive axis: first, a drag-free control loop with one test mass (TM1) where the spacecraft follows TM1 using a micro-propulsion system as an actuation device. Second, a suspension control loop of the other test mass (TM2) where TM2 follows the spacecraft using an electrostatic suspension system for actuation. Clearly, any suspension control activity in the sensitive axis of TM2 has to be performed below the MBW.

For the suspension control of TM2, there are basically two options: it can either be suspended with respect to the spacecraft or with respect to TM1. These options are denoted as M1 and M3, respectively. M1 is the nominal mode.

In M1, the steady state measurement O_{Laser} can be expressed in a simplified manner as follows, see [1, 2]:

$$O_{\text{Laser}} = \frac{1}{s^2}\left[\frac{f_{x2} - f_{x1}}{m} + \left(\omega_{lfs}^2 + \omega_{p2}^2 - \omega_{p1}^2\right) x_1\right].$$

Here, 's' is the Laplace transformation variable. In the brackets, the following two terms can be identified that must be kept small:

- Acceleration due to (total) stiffness $\left(\omega_{lfs}^2 + \omega_{p2}^2 - \omega_{p1}^2\right)x_1$.
  x_1 is the displacement of TM1 along the sensitive axis with respect to the optical bench. ω_{lfs}^2 is the proportional feedback gain of the suspension control. ω_{p1}^2 and ω_{p2}^2 are the parasitic stiffness of TM1 and TM2, respectively, which are mainly caused by a self-gravity gradient (see also figure 2 for an illustration of the effect). Both ω_{lfs}^2 and ω_{p2}^2, ω_{p1}^2 can be considered as 'springs' with positive and negative stiffness, respectively.
- 'Direct' differential force per unit mass $(f_{x2} - f_{x1})/m$.
  f_{x2}/m and f_{x1}/m are forces per unit mass that are applied 'directly' on the test masses 2 and 1, respectively. This term contains contributions that originate from actuation noise, magnetic and thermal, self-gravity, random charging, etc and from actuation and stiffness coupling effects from cross-axes.

Concerning the control system design, it can be concluded that the drag-free bandwidth has to be relatively large (to keep x_1 small), and the suspension bandwidth has to be relatively small (to keep ω_{lfs}^2 small). Furthermore, any stiffness and actuation cross-talk effects from the cross-axes control loops have to be minimized.

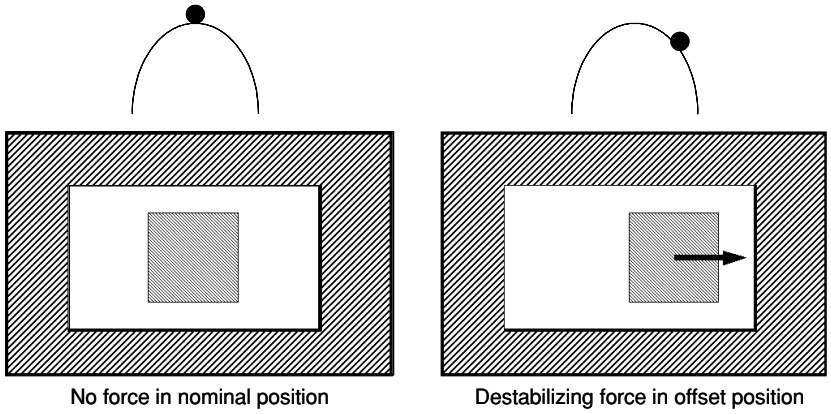


Figure 2. Illustration of negative stiffness effect.

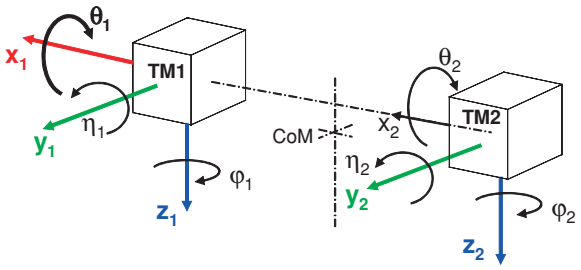


Figure 3. Selection of drag-free coordinates.

Due to the self-gravity gradient, any offset position from an ideally balanced system yields a larger force which accelerates the proof mass away from its nominal position.

1.2. Control tasks

In addition to the control of TM1 and TM2 along the sensitive axis, cross-axis coordinates have to be controlled. The complete control problem for LISA Pathfinder can functionally be specified as follows:

1. Drag-free control in the coordinate x_1 and five additional cross-axes coordinates (y_1, z_1, y_2, z_2 and θ_1) in order to reduce the stiffness cross-coupling effects. A maximum of six coordinates can be drag-free controlled with the micro-propulsion system.
2. Suspension control in the coordinate x_2 and five additional cross-axes coordinates (η_1, ϕ_1, θ_2, η_2 and ϕ_2). This is required in order to stabilize the system.
3. Attitude control of the spacecraft with respect to the inertial reference system, in order to obtain proper thermal and power conditions (Sun pointing).

The definition of the coordinates is shown in figure 3. The total 15 control coordinates are fairly coupled, which complicates the control design. Note that the control problem for the so-called joint operations mode (the LTP and the disturbance reduction system, a second LTP-like instrument with two test masses, are controlled at the same time) is very similar; simply the choice of drag-free coordinates is more special. The same is true for the LISA control problem.

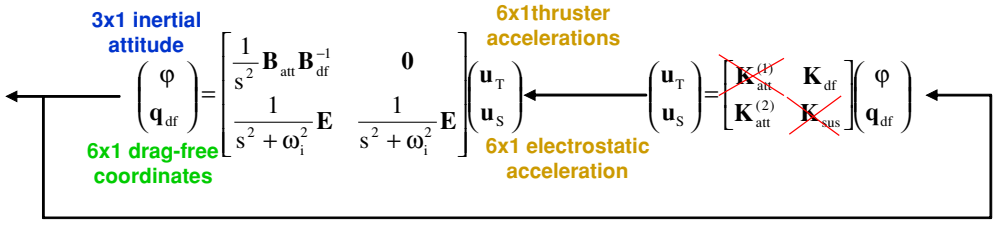


Figure 4. Decoupled design plant and feedback control structure.

2. Feedback control structure and design procedure

The control design consists of two steps: a feedback interconnection that yields a system of decoupled simple single-input–single-output (SISO) systems, and a control design procedure for the SISO systems that allows for the assignment of closed-loop performance characteristics. The consideration/specification of closed loops and simple SISO systems facilitate considerably the system engineering design process.

The *coordinate decoupling* is presented for attitude and drag-free control. Extension to additional suspension control is straightforward. Appropriate rearrangement of the equations of motion yields a fairly decoupled system as shown in figure 4 (left-hand side). Here $\boldsymbol{\varphi}$ is the 3×1 inertial attitude vector, $\mathbf{q}_{\mathrm{df}}$ is the 6×1 vector of drag-free coordinates, $\mathbf{u}_{\mathrm{T}}$ is the 6×1 actuation vector of thrusters (each element of $\mathbf{u}_{\mathrm{T}}$ is realized by an appropriate linear combination of thrusters) and $\mathbf{u}_{\mathrm{s}}$ is the 6×1 actuation vector of the electrostatic suspension on the drag-free axes. $\mathbf{E}$ is the unit matrix, $\mathbf{B}_{\mathrm{att}}$ and $\mathbf{B}_{\mathrm{df}}$ are matrices that contain geometrical properties (nominal test mass positions with respect to the centre of mass) [4]. The ω_i^2 represent the parasitic stiffness of each drag-free axis.

Drag-free coordinates can be actuated individually and are fully decoupled from each other. However, there are still two remaining undesired 'coupling' effects: first, any actuation on the drag-free coordinates with thrusters results in an actuation of the attitude motion. Second, attitude coordinates cannot be actuated individually.

The most general feedback control structure is illustrated in figure 4 (right-hand side). The analysis of the closed-loop transfer functions yields the following results.

1. $\mathbf{K}_{\mathrm{att}}^{(1)}$ and $\mathbf{K}_{\mathrm{df}}$ are in conflict, because both of them rely on the same actuation device. Therefore, $\mathbf{K}_{\mathrm{att}}^{(1)}$ is set to zero.
2. The suspension control $\mathbf{K}_{\mathrm{sus}}$ appears as the sum $(\mathbf{K}_{\mathrm{df}} + \mathbf{K}_{\mathrm{sus}})$ only. This is obvious since both $\mathbf{K}_{\mathrm{df}}$ and $\mathbf{K}_{\mathrm{sus}}$, have the same purpose. Therefore, $\mathbf{K}_{\mathrm{sus}}$ is set to zero.
3. With a closed drag-free control loop, the plant dynamics for the attitude control results in

$$\begin{aligned}\varphi &= -\frac{1}{s^2}\mathbf{B}_{\mathrm{att}}\mathbf{B}_{\mathrm{df}}^{-1}\mathbf{K}_{\mathrm{df}}(\mathbf{E} + (\mathbf{E}s^2 + \boldsymbol{\Omega}^2)^{-1}\mathbf{K}_{\mathrm{df}})^{-1}(\mathbf{E}s^2 + \boldsymbol{\Omega}^2)^{-1}\mathbf{u}_{\mathrm{S}} \\ &\approx -\frac{1}{s^2}\mathbf{B}_{\mathrm{att}}\mathbf{B}_{\mathrm{df}}^{-1}\mathbf{u}_{\mathrm{S}}.\end{aligned}$$

This is a simple double integrator system. $\boldsymbol{\Omega}^2$ is the stiffness matrix. The matrix $\mathbf{B}_{\mathrm{att}}\,\mathbf{B}_{\mathrm{df}}^{-1}$ is 'flat' and thus, a pseudo-inverse $\left(\mathbf{B}_{\mathrm{att}}\,\mathbf{B}_{\mathrm{df}}^{-1}\right)^{I}$ can be introduced in the controller for further decoupling. The nullspace can be exploited for implementing rotations around specific points, e.g. TM1, TM2 or any point on its connection line.

The major advantage of the feedback control interconnection described above is that the total system results in three sets of SISO systems, while preserving the dynamical properties of

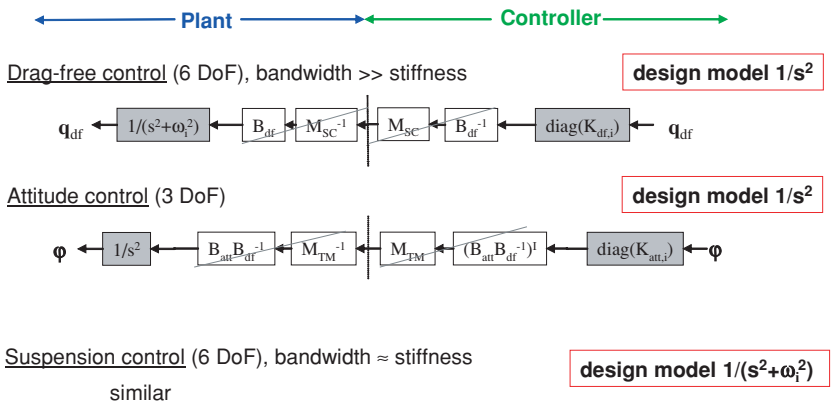


Figure 5. Three sets of simple SISO design models for drag-free, attitude and suspension control.

the drag-free and suspension coordinates. Therefore, the design and analysis can be performed on SISO systems without introducing conservative assumptions with respect to the original coupled system. The design plants are extremely simple, which is illustrated in figure 5.

The *controller design procedure* for the SISO systems is based on H_∞ closed-loop shaping methods [4]. This allows not only the optimization of spectral densities rather than RMS, but also a simple mapping of the spectral density requirements on accelerations, displacements, etc into closed-loop transfer function requirements, and the detection of requirement inconsistencies before the actual design.

3. System performance

3.1. Mode M1 and stability limitation

On the basis of the requirements and constraints for LISA Pathfinder [3], a closed-loop performance analysis is performed in both the time and frequency domain. Typical results are depicted in figures 6 and 7. All performance requirements (lower bounds of the shaded regions) can be met for the relative coordinate control accuracies, as well as the total differential acceleration. Note that the requirements on the relative coordinates are also relaxed with $[1 + (f/3\ \mathrm{mHz})^2]$ in order to minimize the drag-free control bandwidth.

In all the axes, gain/phase margins better than 6 dB/30° can be achieved, with one exception—the suspension control loop of TM2 along the sensitive axis. On this axis, the gain/phase margins are 0.6 dB and 6°, which is not acceptable.

The reason for this limitation is the unstable pole of the plant dynamics at about 2×10^{-4} Hz. This pole requires a minimum control gain. On the other hand, in the MBW, the control gain is required to be below a maximum value. Therefore, the closed-loop frequency response roll-off must be extremely 'fast'. This leads to an overshoot of the closed-loop frequency, corresponding to small stability margins. The frequency domain overshoot is shown in figure 8. In the case of a second-order roll-off rate of the complementary sensitivity function T, the relation between the overshoot M_T of T with respect to the 0 dB line and the 0 dB cross-over frequency ω_T is given by

$$\omega_T > p\sqrt{\frac{M_T}{M_T - 1}}$$

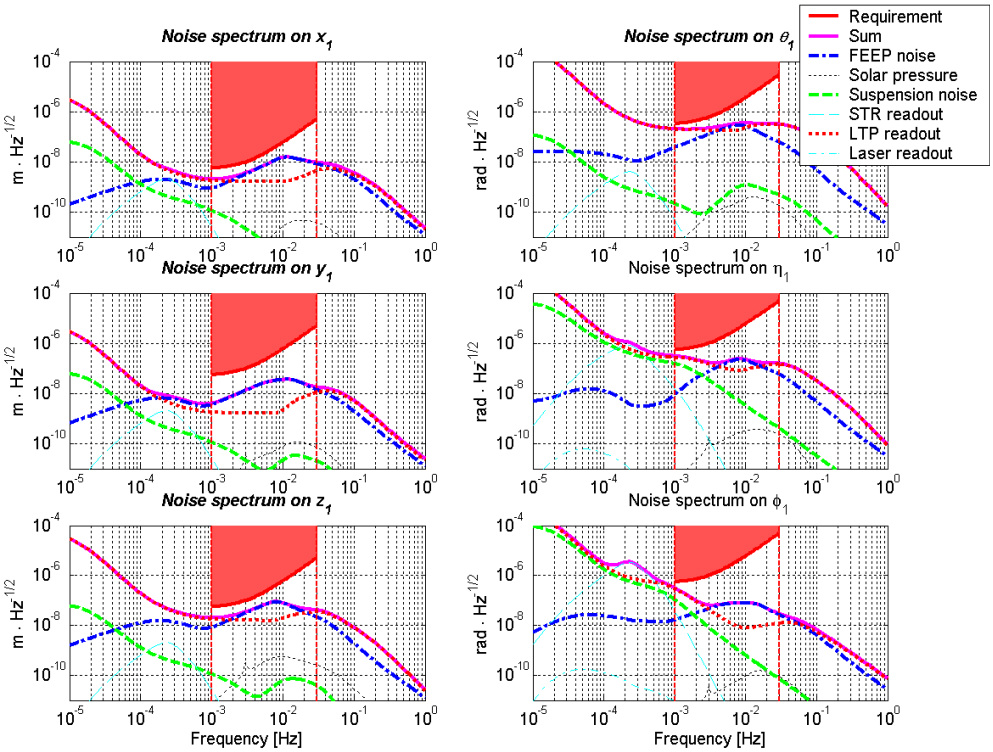


Figure 6. Typical performance results for coordinates of test mass 1. 'STR' denotes 'star tracker', the sensor that measures 3-axis inertial attitude. 'FEEP' stands for 'field emission electric propulsion', i.e. the micro-propulsion system that provides thrust for force/torque generation.

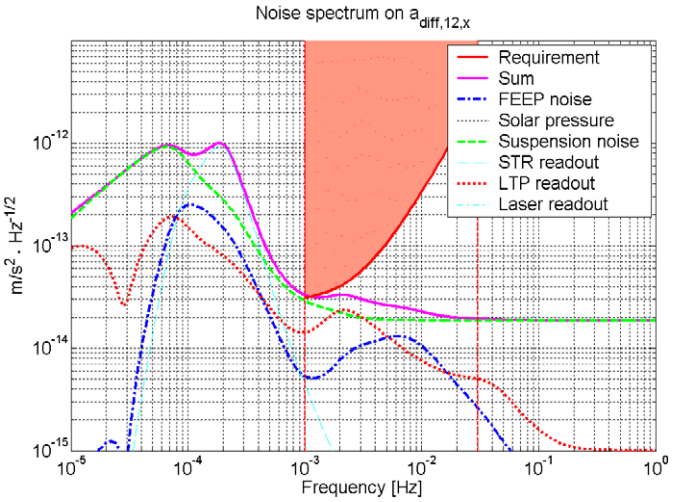


Figure 7. Differential acceleration between the test masses.

where p is the unstable pole. The only way to cope with this situation in mode M1 (assuming all the parameters and the uncertainties remain unchanged) is to approach the stability limits

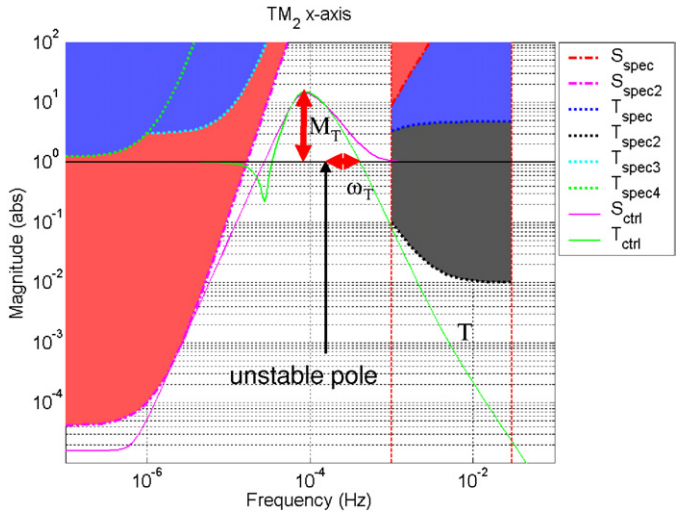


Figure 8. Closed-loop transfer functions S and T for TM2 suspension control along the sensitive axis.

in the actual experiment as close as possible. An alternative to mode M1 is mode M3, which is explained in the next section.

3.2. Mode M3

In mode M3, the test mass 2 is suspended with respect to test mass 1 rather than with respect to the spacecraft (optical bench). This leads to a different steady-state measurement equation. It is given by (simplified version)

$$O_{\text{Laser}} = \frac{1}{s^2 + \omega_{lfs}^2}\left[\frac{f_{x2} - f_{x1}}{m} + \left(\omega_{p2}^2 - \omega_{p1}^2\right)x_1\right].$$

The terms to be measured in the brackets are independent of the suspension control gain ω_{lfs}^2. ω_{lfs}^2 only affects the 'filter function' of the measurement, i.e. it alters the behaviour with respect to $1/s^2$ behaviour. This effect can be removed by post-processing, and, therefore, the suspension control gain may be larger compared to M1. This eliminates the stability robustness issue addressed for M1.

In figure 9, the acceleration performance for mode M3 is shown. In figure 10, it is shown that the gain and phase margins remain within the specifications even with uncertain gain and stiffness.

3.3. Major contributions to differential acceleration

In mode M1, the total acceleration at 1 mHz is 31×10^{-15} m s^{-2} Hz$^{-1/2}$. The sensitive axis accelerations are mainly 'direct forces'. Contributions from the control system can be kept within 14.7×10^{-15} m s^{-2} Hz$^{-1/2}$. The most significant cross-coupling contribution is originated by actuation cross-talk, in the order of 12×10^{-15} m s^{-2} Hz$^{-1/2}$. This contribution depends significantly on the actuation cross-talk coefficients.

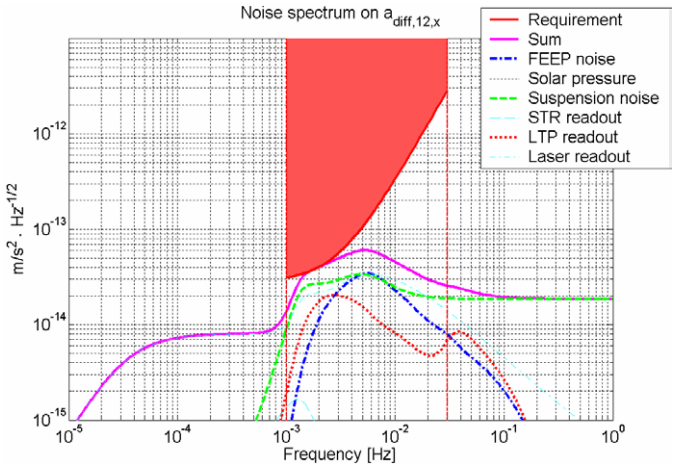


Figure 9. Acceleration performance in M3.

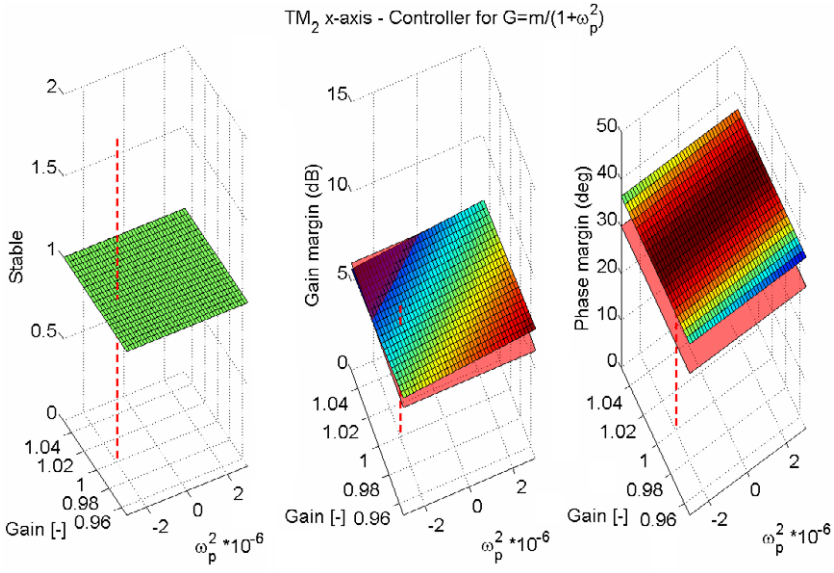


Figure 10. Gain/phase margins with stiffness uncertainty in mode M3. Left plot: '1' denotes 'stable'.

Table 1. Top-level differential acceleration noise budget for mode M1.

	'Direct' acceleration noise $(f_2 - f_1)/m$	Stiffness $(\omega_2^2 - \omega_1^2 + \omega_{ifs}^2)x_10$	Stiffness cross-talk	Actuation cross-talk	Quadratic sum
$\times 10^{-15}$ m s^{-2} Hz$^{-1/2}$	28	8.12	1.05	12.3	31.0

A top-level acceleration noise budget is summarized in table 1. The values are given at the lower bound of the measurement bandwidth, i.e. 1 mHz.

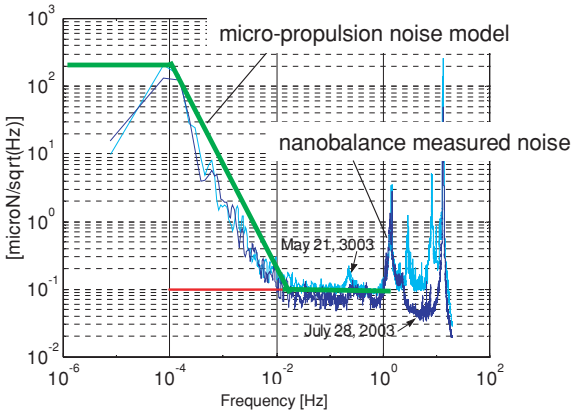


Figure 11. Thrust balance noise (without thrust noise) and thruster noise model. Measurement: courtesy of Alenia Spazio.

4. Miscellaneous control system design issues

Sampling frequency. The fastest closed-loop bandwidth is in the order of 0.2 Hz. A rule of thumb requires a sampling frequency to be a factor of 20 times faster (4 Hz). With some margin, a sampling frequency of 10 Hz is selected.

Controller order. The typical controller order of SISO controller is five. This is not a driver for the processor load.

Delay. The drag-free control bandwidths of the closed loops are up to 0.2 Hz. A total delay of 300 ms is considered for design purposes, where 50 ms is allocated for any data processing filtering, including anti-aliasing. This must be considered properly in the design of the optical metrology system and the electrostatic read-out.

Micro-propulsion force noise. The controller design is based on a noise model as shown in figure 11. This is basically an envelope of the thrust balance performance. This means that the model is compatible not only with the thruster specification but also with the thrust noise verification capabilities.

Micro-propulsion actuation algorithm and maximum thrust. The algorithm that distributes the commanded force/torque vector to individual thruster forces consists of standard linear programming and a backup solution based on a pseudo-inverse approach with scaling of the required force/torque vector if necessary. This ensures that a solution is found always within a limited time. Analysis/simulations have shown that the backup algorithm is used typically less than 1%.

Nominally, 12 thrusters are used to generate the force/torque vector demanded by the control system. In the nominal case, i.e. when all 12 thrusters are operational, the maximum force of an individual thruster is typically less than 30 μN. When one thruster fails, its function will be replaced by (a subset of) the remaining 11 thrusters. This leads to a higher maximum force for an individual thruster, typically less than 80 μN.

5. Conclusion

A rather generic control design approach can be used for LISA Pathfinder. This approach is also applicable to the Joint Operations Mode and (with some modifications) to LISA. It allows

the consideration of simple single-input–single-output systems for performance requirements specification and design tasks.

It can be shown that the performance requirements can be met. However, in mode M1 there are extremely (unrealistically) small robustness margins that cannot be improved due to the given design constraints. In M1, the task of the mission is to approach these limits as close as possible. The problem of small robustness can be completely eliminated in the mode M3.

The design of the science mode is compatible with practical control system constraints, in particular, computer load, thruster noise verification capability, maximum thrust and control loop transport delay.

References

[1] Vitale S *et al* 2004 *Science Requirements and Top-Level Architecture Definition for the LISA Test Flight Package* LTPA-UTN-ScRD-Iss2-Rev1 26 April

[2] Vitale S *et al* 2002 LISA and its in-flight test precursor SMART-2 *Nucl. Phys.* B **110** 209–16

[3] Fichter W 2004 *DFACS Requirements Specification* S2-ASD-RS-2001 version 1.1, EADS Astrium GmbH, 13 August

[4] Fichter W and Gath P 2004 *DFACS General Design* S2-ASD-TN-2001 version 1.1, EADS Astrium GmbH, 6 October